

Article

Active Optical Tuning of Azopolymeric Whispering Gallery Mode Microresonators for Filter Applications

Gabriel H. A. Jorge ^{1,2}, Filipe A. Couto ², Juliana M. P. Almeida ³, Victor A. S. Marques ², Marcelo B. Andrade ^{2,4} 
and Cleber R. Mendonça ^{2,*} 

¹ Department of Materials Engineering, School of Engineering of Sao Carlos, University of São Paulo, P.O. Box 359, São Carlos 13563-120, SP, Brazil

² São Carlos Institute of Physics, University of São Paulo, P.O. Box 369, São Carlos 13560-970, SP, Brazil

³ Department of Materials Engineering (DEMa/UFSCar), Federal University of São Carlos, São Carlos 13565-905, SP, Brazil

⁴ Physics Department, Federal University of Ouro Preto, Ouro Preto 35400-000, MG, Brazil

* Correspondence: crmendon@ifsc.usp.br; Tel.: +55-16-3373-8085

Abstract: Light confinement provided by whispering gallery mode (WGM) microresonators is especially useful for integrated photonic circuits. In particular, the tunability of such devices has gained increased attention for active filtering and lasering applications. Traditional lithographic approaches for fabricating such devices, especially Si-based ones, often restrict the device's tuning due to the material's inherent properties. Two-photon polymerization (2PP) has emerged as an alternative fabrication technique of sub-diffraction resolution 3D structures, in which compounds can be incorporated to further expand their applications, such as enabling active devices. Here, we exploited the advantageous characteristics of polymer-based devices and produced, via 2PP, acrylic-based WGM hollow microcylinders incorporated with the azoaromatic chromophore Disperse Red 13 (DR13). Within telecommunication range, we demonstrated the tuning of the microresonator's modes by external irradiation within the dye's absorption peak (at 514 nm), actively inducing a blueshift at a rate of 1.2 nm/(Wcm⁻²). Its thermo-optical properties were also investigated through direct heating, and the compatibility of both natural phenomena was also confirmed by finite element simulations. Such results further expand the applicability of polymeric microresonators in optical and photonic devices since optically active filtering was exhibited.



Citation: Jorge, G.H.A.; Couto, F.A.; Almeida, J.M.P.; Marques, V.A.S.; Andrade, M.B.; Mendonça, C.R. Active Optical Tuning of Azopolymeric Whispering Gallery Mode Microresonators for Filter Applications. *Photonics* **2024**, *11*, 167. <https://doi.org/10.3390/photronics11020167>

Received: 11 January 2024
Revised: 1 February 2024
Accepted: 6 February 2024
Published: 9 February 2024



Copyright: © 2024 by the authors. Licensee MDPI, Basel, Switzerland. This article is an open access article distributed under the terms and conditions of the Creative Commons Attribution (CC BY) license (<https://creativecommons.org/licenses/by/4.0/>).

Keywords: tunable optical microresonators; two-photon polymerization; whispering gallery mode; thermo-optic coefficient; thermal expansion; optical filter

1. Introduction

Ultrashort laser processing of materials, enabling precise patterning of both two-dimensional (2D) and three-dimensional (3D) micro/nanostructures, has become a fundamental technology with widespread applications in academic research and engineering [1]. One extensively utilized technique within ultrashort laser-based fabrication is direct laser writing through two-photon polymerization (2PP) [2]. In contrast to traditional micro/nanofabrication methods, 2PP stands out as a maskless patterning tool that operates without the need of stringent processing conditions or the use of cleanrooms [3]. Leveraging the nonlinear nature of two-photon absorption, 2PP excels in fabricating 3D polymeric microstructures featuring arbitrary geometries and sub-diffraction features [4]. Such arbitrary shapes achieved by 2PP can be very useful for integrated photonics, enabling the fabrication of structures that can be very challenging to achieve in Si-based techniques.

The spatial confinement achieved through 2PP, which enables the fabrication of 3D microstructures, stems from the nonlinear nature of the two-photon absorption (2PA) phenomenon. This 2PA phenomenon involves an electronic transition excited by the combined action of two photons [5], where the sum of the energy of the individual photons

must resonate with the transition energy [3]. The 2PP technique harnesses high-intensity pulsed lasers, leading to the observation of multi-photon absorption phenomena in the irradiated area. Hence, polymerization of small volumes (referred to as voxels) occurs only near the focal spot, granting the fabricated structure finer resolution, below the diffraction limit [6]. By moving the laser beam within the sample, the fabrication of three-dimensional structures becomes feasible without shape limitations, enabling the creation of intricate contours.

The versatility of 2PP extends to its wide suitability for a diverse range of materials as photoresists and their incorporation with specific functional materials, allowing for the tailoring of the physical, chemical, or biological properties of microstructures for different applications [7,8]. These applications extend across various domains, encompassing photonics [9–13], biosciences [13–15], and micromechanical systems [16,17]. Within the realm of photonics, 2PP has been instrumental in the precise fabrication of photonic crystals [18], waveguides [19], photonic wire bonding [20], free-form coupling elements [9], and optical microresonators [21]. Furthermore, 2PP has demonstrated its capability in the fabrication of active photonic structures [20–23]. The advantageous features of 2PP, which include the precise tuning of structure dimensions and the seamless integration of fabricated structures into various substrates, as well as its material versatility, have significantly advanced the design possibilities and potential applications in photonics. Furthermore, 2PP's material flexibility, coupled with its 3D capability and gentle processing conditions, renders it highly suitable for such applications.

Over the past few years, femtosecond laser-induced 2PP has emerged as an alternative method for fabricating Whispering Gallery Mode (WGM) microresonators. In addition to its advantages in resolution and geometry versatility, 2PP offers the capability to incorporate various materials into the polymeric matrix, including organic dyes and nanoparticles. This feature expands the potential applications of microresonators. The direct writing of high-performance polymeric microrings using 2PP was showcased in 2008 [24]. Subsequently, this method has enabled the fabrication of high-Q microresonators in hybrid materials [25,26] and in resins incorporating functional materials [23,27]. Despite these advancements, there is still a demand for the development of active polymeric WGM microresonators, whose properties can be controlled by external means.

Active WGM resonators fabricated in inorganic materials have been successfully demonstrated, achieving tunability through mechanisms such as mechanical stretching, electrical field interaction, heating, direct changing of pressure and refractive index, as well as nonlinear light effects—all of which have been induced in both monolithic and coated microresonators [28–33]. Such active devices can have broad applications in photonic circuits. Real case examples include “IOU” geometries, such as those produced by Li et al. [24] In this case, when large band light is coupled into the system, most of its multiple frequencies are discarded, but selected ones are confined within the resonator to couple into the output. The integration of an active resonator permits the dynamical tuning of the output frequencies, which can be useful for optical filtering applications in diverse fields such as telecommunications, spectroscopy, and imaging.

Despite these achievements and promising applications, the fabrication of inorganic resonators pose significant challenges, particularly when incorporation of compounds is required to enhance desired effects, which typically involves a series of complex chemical and thermal treatments. Achieving a broader tuning range can be also difficult for such devices due to their typical low expansion coefficient [34]. Alternatively, many works achieved tuning in the order of 10^2 nm by exploring QBIC resonances [35–37]; however, they employed phase change materials and liquid crystals. To the best of our knowledge, optically active WGM Si-based devices have been achieved using azobenzene monolayers [33] with a maximum 4 nm blueshift. As far as the authors are aware, analogous optically active devices had not been produced using 2PP or even polymeric materials. Therefore, the ease of incorporating compounds into polymeric microstructures, such as

WGM resonators, presents a promising alternative to be explored in order to overcome the challenges of inorganic platforms to produce optically active devices.

Here, 2PP was used to manufacture high-Q WGM acrylic-based polymeric hollow microcylinders containing the azoaromatic chromophore Disperse Red 13 (DR13) in order to tune the microresonators resonances by external light excitation at 514 nm, which is resonant with DR13 absorption. The microresonators were optically coupled through the evanescent field, in the telecommunication range, using tapered optical fibers. The mode tuning, resulting from thermo-optical effects caused by the DR13 absorption, was investigated as a function of the external light irradiance, and the results were interpreted using finite elements simulations.

2. Materials and Methods

For the 2PP fabrication, a Ti:Sapphire oscillator emitting 100-fs laser pulses at 780 nm with an 86 MHz repetition rate was employed. Laser intensity modulation was achieved through a half-wave plate and a polarizer. To enhance fabrication resolution, the intensity was finely adjusted near the resist polymerization threshold. The laser beam was focused onto a photoresist sample using a 0.25 NA microscope objective, and the focus position in the x , y planes was manipulated by a pair of galvanometric mirrors. The z position of the sample was controlled by a motorized stage, allowing a layer-by-layer fabrication process. Further details about the fabrication process can be found in other references [6,10]. The undoped photoresist comprised two monomers, dipentaerythritol pentaacrylate (SR399—Sartomer[®], Exton, PA, USA) and tris(2-hydroxy ethyl)isocyanurate triacrylate (SR368—Sartomer[®]), in a ratio of 90/10. Additionally, Irgacure TPO-L was used as a photoinitiator and added at 3% of the total weight. These proportions had been previously optimized [10] to produce structures with good structural quality and low surface roughness. To incorporate DR13 into the photoresist, the dopant was first dispersed in ethanol and subjected to ultrasonication to create a homogeneous solution. This solution was then mixed with the undoped photoresist in a proportion of 1 wt%, and the mixture was subjected to magnetic stirring at 65 °C for 2 hours to ensure the uniform dispersion of the dopant and facilitate ethanol evaporation. Light coupling into the resonators was accomplished using an evanescent wave from a tapered optical fiber, as illustrated in Figure 1a. The fabrication of the taper involved employing two motorized stages that gradually stretched the fiber, while a small flame generated a heat zone in the targeted tapered region. The final diameter of the taper could be adjusted by controlling the amount of stretching [38], aiming for taper diameters of approximately 3 μm . To bring the tapered fiber into contact with the resonator, translational stages were employed to control the x , y , z positions of both the tapered optical fiber and the substrate containing the resonators. Furthermore, the rotation of the taper was also controlled in order to ensure orthogonal positioning concerning the z -axis of the resonators, minimizing the presence of spiral leaky modes. The entire process was monitored using a stereo microscope coupled with a CCD camera.

To access the resonant modes of the structures, the tapered fiber was coupled to a high-resolution tunable semiconductor laser source, and the output power was continuously monitored using a diode photodetector. Initially, a calibration run was conducted by sweeping the laser source across the spectral region of interest while the tapered fiber was positioned far from the resonator. This step allowed for the measurement of the uncoupled transmission spectra of the system. Subsequently, the tapered optical fiber was brought into close proximity to the resonator, and a second sweep was performed. The transmittance spectrum of the coupled system was then defined as the ratio of the coupled run to the calibration run, where the resonant modes of the resonator appeared as sharp Lorentzian dips.

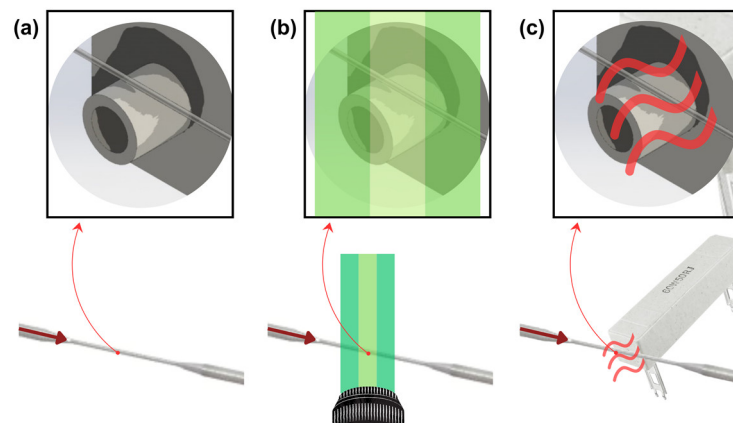


Figure 1. (a) Illustration of the evanescent coupling of the resonator using a tapered optical fiber. (b) External excitation of the WGM resonator using an Ar-ion laser at 514 nm. (c) Schematic representation of heating the microresonator using a ceramic resistor.

To actively change the resonances of the microstructure by thermo-optical effects, a 514 nm line from an Ar-ion laser was directed towards the resonator, perpendicular to its z-axis, as displayed in Figure 1b. Laser intensity was controlled using a polarizer and a half-wave plate. The laser beam spot diameter was approximately 3 mm, ensuring that the entire structure experienced relatively uniform laser irradiation. Alternatively, a ceramic resistor was positioned near the resonator, producing heat by Joule effect, as illustrated in Figure 1c. Temperature control was achieved by adjusting the voltage applied to the resistor and was monitored using a thermocouple.

Imaging and optical analysis were also performed on the microstructure. Scanning electron microscopy (SEM) was employed to assess resonator parameters such as height and radius. An auxiliary software integrated into the SEM equipment (3D-Image Viewer Version 2.3) was used to construct a 3D image of the resonators and estimate their surface roughness. The linear absorption spectrum of the doped photoresist was carried out in films approximately 10.5 μm thick, cured under UV light. The absorption spectra were measured using a commercial spectrophotometer SHIMADZUTM UV-1800. The same spectrophotometer was used to estimate the refractive index of the acrylic resin, performing a fitting parametrized by the Sellmeier equation.

For thermodilatometry measurements of the photoresist, macroscopic samples of both the undoped and doped resists were polymerized into millimetric blocks using either an He-Cd laser source (at 325 nm and 442 nm) or a 15W UV lamp, and the measurements were conducted using 402 C equipment (NETZSCH, Selb, Germany), with temperatures ranging from 20 $^{\circ}\text{C}$ to 110 $^{\circ}\text{C}$ at a rate of 7 $^{\circ}\text{C}/\text{min}$.

The finite element software COMSOL Version 5.6, using the “Heat Transfer in Solids” module, was employed to simulate the expected thermomechanical behavior of the fabricated resonators. The structures were modeled as 67 μm tall cylinders, with an external radius of 26.7 μm and an internal radius of 16.7 μm . One of the faces along the z-axis was constrained to a fixed size, simulating attachment to the substrate. The remaining portion of the cylinders was left free to undergo thermal expansion. The expansion coefficient was used from the thermodilatometry measurements ($4.3 \times 10^{-5}/^{\circ}\text{C}$), while density values were determined as the weighted mean values of the monomers, as provided by the vendor [39].

3. Results and Discussion

A SEM micrograph of a typical microresonator produced via 2PP is depicted in the inset of Figure 2. The device measures approximately 85 μm in height, featuring a diameter of 53 μm and walls that are 10.5 μm thick. A surface roughness of at most 15 nm was

estimated with the SEM equipment's 3D analysis software, indicating that the resonators are suitable for applications in the near-infrared spectral region.

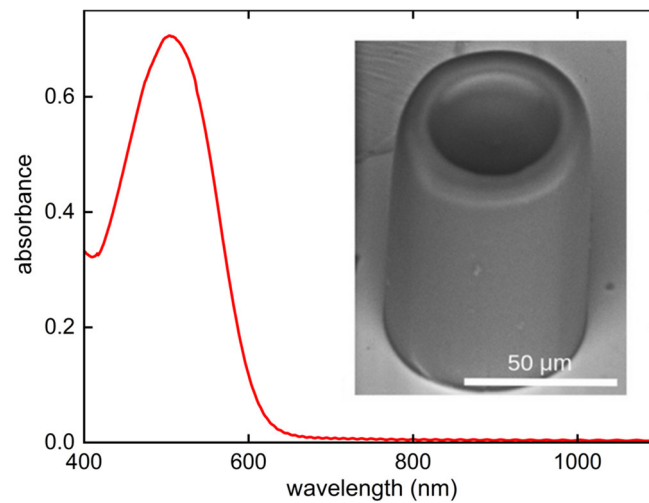


Figure 2. Absorption spectra of a 15 μm thick polymerized film doped with DR13. The inset displays a SEM micrograph of a microresonator sharing the same composition, fabricated by direct femtosecond laser writing via 2PP.

The absorption spectrum of the doped photoresist, depicted in Figure 2, shows an absorption peak near 514 nm, attributed to DR13 [40], and a broad transparency window in the near-infrared region, which is a known feature of this photoresist [41]. From the sample absorbance at 514 nm, we were able to determine the linear absorption coefficient of the resist as $\alpha = 1070 \text{ cm}^{-1}$. Considering the wall thickness and neglecting fluorescence from the DR13, it is expected that 95% of the energy from a laser source incident perpendicularly on the resonator will be absorbed and converted into thermal energy.

Figure 3a displays the microresonator's spectra collected over seven minutes. No changes in the modes' spectral positions were observed over time (shift was smaller than 0.1 nm), confirming the spectrum stability when no external irradiation was applied. Also, from the consecutive azimuthal modes identified in the spectrum, we determine the resonator's free spectral range (FSR) as 9.3 nm. Using $\text{FSR} = \frac{\lambda^2}{2\pi a n}$, in which λ is the mode wavelength, a is the resonator's radius, and n is its index of refraction (considered here to be $n = 1.54$), we determined that the FSR = 9.13 at 1530 nm, which is in good agreement with the observed experimental one.

An asymmetric Lorentzian fit was used to determine the Q-factor of the resonances [25], as shown in Figure 2. The Q-factor is described by $Q = \lambda_0 / \Delta\lambda$, correlating the resonance wavelength (λ_0) and its linewidth ($\Delta\lambda$). Using $\Delta\lambda = 21 \text{ pm}$, determined from the fitting, we calculated that $Q = 7.1 \times 10^4$ for the deepest resonance ($\sim 1516 \text{ nm}$). It is important to note that the incorporation of DR13 did not negatively affect the microresonator's light confinement, since the Q-factor values observed here are in the same order as those observed for other polymeric microresonators previously reported [8,25], which reinforces 2PP's advantages of incorporating different organic compounds to obtain distinct properties without needing additional post-processing steps.

As can be seen in Figure 4a, a blueshift of the modes is observed when the microresonator is irradiated at 514 nm (as illustrated in Figure 1b), correlated with the laser irradiance. Specifically, for the resonance located at 1515.8 nm, a maximum blueshift of 0.8 nm was achieved for the higher irradiance employed (0.67 W/cm^2). To ascertain the reversibility of this process, we initiated the resonator excitation with the higher irradiance and systematically decreased it. As shown in Figure 4b, the spectrum reverted to its initial position (without external irradiation), within the experimental error. Figure 4c displays the resonance shift as a function of the external laser irradiance when it is increased (blue) and

decreased (red). The data reveal an approximately linear relationship, with a slope of about $-1.2/(W\text{cm}^{-2})$. The observed shift in the microstructure resonances is associated with thermal-induced changes in the resonator's radius and refractive index upon excitation with the Ar-ion laser.

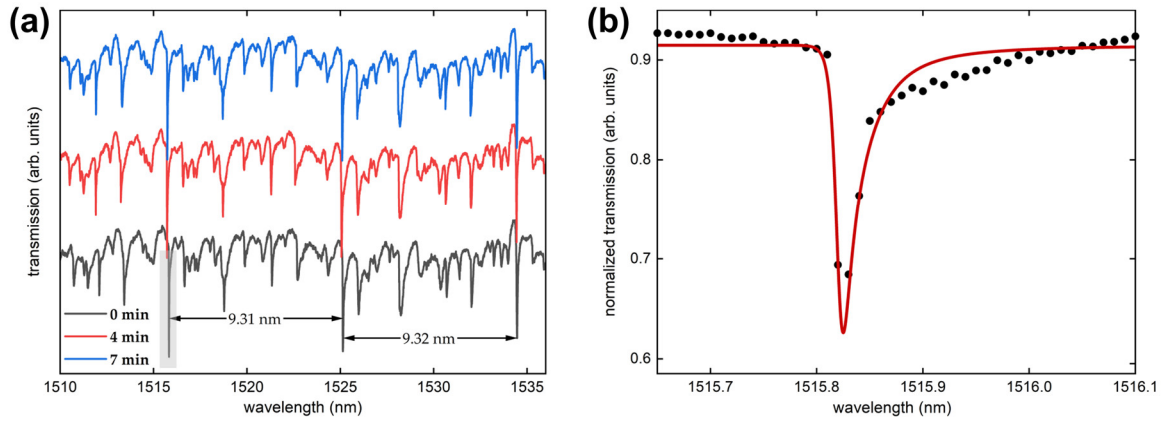


Figure 3. (a) Transmission spectra of a 2 μm waist taper coupled to a DR13-doped polymeric microresonator for seven minutes. The free spectral range values of ~ 9.3 nm are displayed. (b) Zoom-in at the deepest resonance (shaded in part a) along with the Q-factor and full width half maximum obtained by fitting.

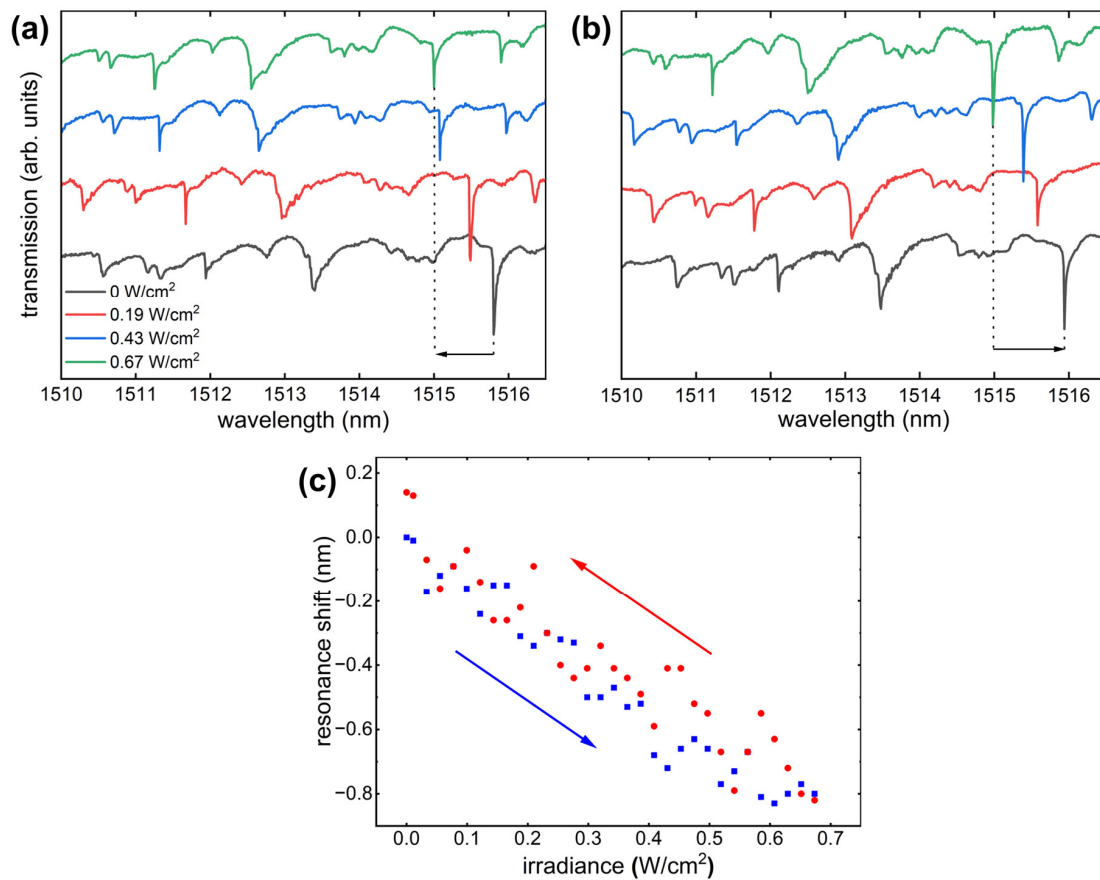


Figure 4. Transmission spectra of the DR13-doped polymeric microresonator for increasing (a) and decreasing (b) external irradiances (Ar-ion laser at 514 nm). (c) Resonance (1515.8 nm) shift as a function of the external laser irradiance increase (blue) and decrease (red). The blue and red arrows are guides to the eye, respectively, for increasing and decreasing irradiation.

Before further discussing the thermo-optical processes leading to the modes' frequency shifts, we performed a direct temperature change experiment on the resonator to study the magnitude of thermal effects. Similarly, multiple spectra were captured, and the position of a resonance peak (1519 nm at room temperature) was tracked for each different temperature in the range of 30–44 °C. As seen in Figure 5, we observed a blueshift of the spectra when the temperature increases and a redshift when it decreases, reinforcing the thermal nature of the phenomenon previously induced by the Ar-ion laser. A linear fit of the dataset yielded a slope of $-0.2 \text{ nm}/^\circ\text{C}$. Relating it with the slope previously obtained in the irradiation experiment, one can estimate that each 1 Wcm^{-2} of irradiance can induce a heating of approximately $6 \text{ }^\circ\text{C}$ in the microresonator.

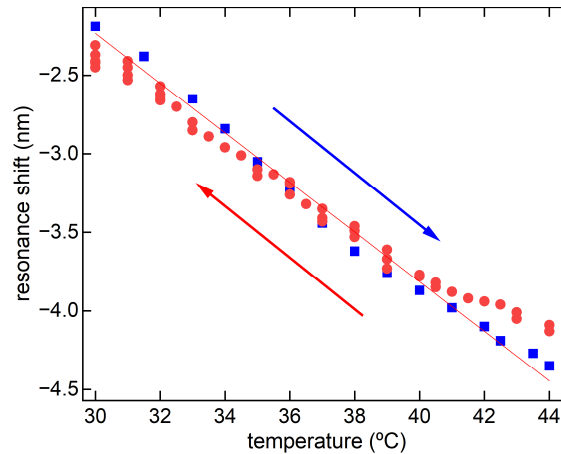


Figure 5. Resonance (1519.47 nm) shift as a function of the temperature increase (blue) and decrease (red). The blue and red arrows are guides to the eye, respectively, for increasing and decreasing temperature.

The spectral dependency of the WGM's resonance shift with the temperature can be modeled as [42–45]:

$$\Delta\lambda/\Delta T = \lambda(\delta + \beta) \tag{1}$$

where the wavelength shift ($\Delta\lambda$) for a given temperature shift (ΔT), at an initial resonance wavelength (λ), is described by two intrinsic characteristics of the material: its linear expansion coefficient (δ) and its thermo-optic coefficient (dn/dT , being $\beta = n^{-1}dn/dT$).

Dilatometry of the cured doped photoresist was performed, yielding the value $\delta = (4.3 \pm 0.1) \times 10^{-5}/^\circ\text{C}$. Rewriting Equation (1) as:

$$\Delta\lambda = \lambda \left(\delta + \frac{1}{n} \frac{dn}{dT} \right) \Delta T \tag{2}$$

the thermo-optic coefficient of the material can be obtained by a linear fit of the data presented in Figure 5 (solid line), revealing the value of $dn/dT = (2.36 \pm 0.03) \times 10^{-4}/^\circ\text{C}$. Since, to the best of our knowledge, there are no data available for this specific doped photoresist, we highlight that the results are in the same order of magnitude as those found in the literature for PMMA, which is also an acrylic material [46,47].

Additionally, we performed a finite element method (FEM) simulation of the radial displacement of the resonator when irradiated by a heat source coming from one side of its external walls (Figure 6a). This simulation was performed to ensure that there was no significant difference due to a possible asymmetric heating, which could lead to an incompatibility of the results obtained by laser irradiation and resistor heating. As shown in Figure 6b, after 3 seconds of heating, there is a $0.1 \text{ }^\circ\text{C}$ difference from one side to another of the cylinder, which is expected to lead to a negligible asymmetry in the radial shape, as confirmed in Figure 6c. The model also considered the constraint of the structure to the substrate, as can be seen in the low radial displacement in the base of the

resonator in Figure 6c. Simulation data, for the same range of temperatures used in the experiments, show that this constraint does not significantly change the radial expansion of the central region of the resonator, which can be considered to behave the same way as a free space structure.

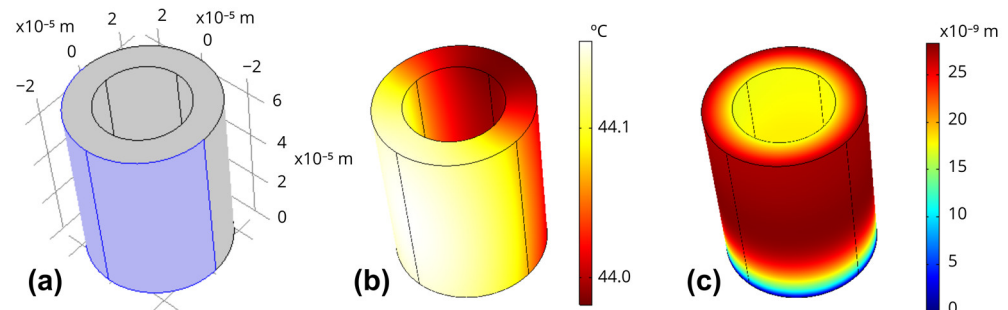


Figure 6. (a) Geometry of a simulated microresonator along with the region in which its heat source from irradiation is defined; (b) temperature map of the resonator submitted to an arbitrary irradiance after transient time; and (c) radial displacement map of the same resonator.

4. Conclusions

Two-photon polymerization was performed to fabricate polymeric WGM microresonators containing azaromatic chromophore Disperse Red 13. Low surface roughness devices were obtained, which presented high-Q WGM modes that can be promising in sensing, filtering, and lasing applications. We have demonstrated the tunability of the resonator's modes by exposing the device to an Ar-ion laser beam, operating at 514 nm. A blueshift of about $1.2/(W\text{cm}^{-2})$ was achieved, which we concluded to be related to thermal optical effects associated with the DR13 absorption. Direct heating of the microresonator helped in understanding the principles of this modal shift, and, together with the dilatometry of the resonator's compound, provided an estimation of the doped polymer's thermo-optic coefficient, consistent with the literature data for similar materials. Ultimately, we verified that our direct heating method induces a symmetrical displacement of the resonator, thus confirming its equivalence with the laser heating method. These findings broaden the potential applications of polymeric microresonators in optical and photonic devices.

Author Contributions: Conceptualization, C.R.M.; Methodology, G.H.A.J. and F.A.C.; Software, G.H.A.J., F.A.C.; Formal analysis, G.H.A.J., F.A.C. and M.B.A.; Investigation, G.H.A.J., F.A.C., J.M.P.A., V.A.S.M. and M.B.A.; Data curation, G.H.A.J.; Writing—original draft preparation, G.H.A.J., F.A.C., J.M.P.A., V.A.S.M., M.B.A. and C.R.M.; Writing—review & editing, G.H.A.J., F.A.C., J.M.P.A., V.A.S.M., M.B.A. and C.R.M.; Supervision, C.R.M.; Funding acquisition, C.R.M. All authors have read and agreed to the published version of the manuscript.

Funding: This research was funded by Fundação de Amparo à Pesquisa do Estado de São Paulo (FAPESP)—Grant numbers: 2017/12174-4, 2018/11283-7, 2020/08715-2, Conselho Nacional de Desenvolvimento Científico e Tecnológico (CNPq)—Grant number: 161761/2021-6, Coordenação de Aperfeiçoamento de Pessoal de Nível Superior—Brasil (CAPES)—Grant number: 001, Air Force Office of Scientific Research (AFOSR) (FA9550-23-1-0664), and the US ARMY (W911NF2110362).

Institutional Review Board Statement: Not applicable.

Informed Consent Statement: Not applicable.

Data Availability Statement: The data underlying the results presented in this article may be obtained from the authors upon reasonable request.

Acknowledgments: The authors thank Kelly T. Paula assisting in the 3D imaging and optical analysis, and André A. Romero for the general technical assistance.

Conflicts of Interest: The authors declare no conflicts of interest.

References

1. Malinauskas, M.; Farsari, M.; Piskarskas, A.; Juodkasis, S. Ultrafast laser nanostructuring of photopolymers: A decade of advances. *Phys. Rep.* **2013**, *533*, 1–31. [[CrossRef](#)]
2. LaFratta, C.N.; Fourkas, J.T.; Baldacchini, T.; Farrer, R.A. Multiphoton fabrication. *Angew. Chem.—Int. Ed.* **2007**, *46*, 6238–6258. [[CrossRef](#)] [[PubMed](#)]
3. Maruo, S.; Nakamura, O.; Kawata, S. Three-dimensional microfabrication with two-photon-absorbed photopolymerization. *Opt. Lett.* **1997**, *22*, 132–134. [[CrossRef](#)] [[PubMed](#)]
4. Kawata, S.; Sun, H.-B.; Tanaka, T.; Takada, K. Finer features for functional microdevices. *Nature* **2001**, *412*, 697–698. [[CrossRef](#)] [[PubMed](#)]
5. Boyd, R.W. *Nonlinear Optics*; Elsevier: Amsterdam, The Netherlands, 2020. [[CrossRef](#)]
6. Otuka, A.J.G.; Tomazio, N.B.; Paula, K.T.; Mendonça, C.R. Two-Photon Polymerization: Functionalized Microstructures, Micro-Resonators, and Bio-Scaffolds. *Polymers* **2021**, *13*, 1994. [[CrossRef](#)] [[PubMed](#)]
7. Sun, H.B.; Kawata, S. Two-photon photopolymerization and 3D lithographic microfabrication. *Adv. Polym. Sci.* **2004**, *170*, 169–273. [[CrossRef](#)]
8. Carlotti, M.; Mattoli, V. Functional Materials for Two-Photon Polymerization in Microfabrication. *Small* **2019**, *15*, 1902687. [[CrossRef](#)] [[PubMed](#)]
9. Dietrich, P.I.; Blaicher, M.; Reuter, I.; Billah, M.; Hoose, T.; Hofmann, A.; Caer, C.; Dangel, R.; Offrein, B.; Troppenz, U.; et al. In situ 3D nanoprinting of free-form coupling elements for hybrid photonic integration. *Nat. Photonics* **2018**, *12*, 241–247. [[CrossRef](#)]
10. Tomazio, N.B.; Otuka, A.J.G.; Almeida, G.F.B.; Roselló-Mechó, X.; Andrés, M.V.; Mendonça, C.R. Femtosecond laser fabrication of high-Q whispering gallery mode microresonators via two-photon polymerization. *J. Polym. Sci. B Polym. Phys.* **2017**, *55*, 569–574. [[CrossRef](#)]
11. Lindenmann, N.; Dottermusch, S.; Goedecke, M.L.; Hoose, T.; Billah, M.R.; Onanuga, T.P.; Hofmann, A.; Freude, W.; Koos, C. Connecting silicon photonic circuits to multicore fibers by photonic wire bonding. *J. Light. Technol.* **2015**, *33*, 755–760. [[CrossRef](#)]
12. Jimenez Gordillo, O.A.; Chaitanya, S.; Chang, Y.-C.; Dave, U.D.; Mohanty, A.; Lipson, M. Plug-and-play fiber to waveguide connector. *Opt. Express* **2019**, *27*, 20305. [[CrossRef](#)] [[PubMed](#)]
13. Pitts, J.D.; Campagnola, P.J.; Epling, G.A.; Goodman, S.L. Submicron multiphoton free-form fabrication of proteins and polymers: Studies of reaction efficiencies and applications in sustained release. *Macromolecules* **2000**, *33*, 1514–1523. [[CrossRef](#)]
14. Tayalia, P.; Mendonça, C.R.; Baldacchini, T.; Mooney, D.J.; Mazur, E. 3D cell-migration studies using two-photon engineered polymer scaffolds. *Adv. Mater.* **2008**, *20*, 4494–4498. [[CrossRef](#)]
15. Gittard, S.D.; Ovsianikov, A.; Akar, H.; Chichkov, B.; Monteiro-Riviere, N.A.; Staflieni, S.; Chisholm, B.; Shin, C.-C.; Shih, C.-M.; Lin, S.-J.; et al. Two photon polymerization-micromolding of polyethylene glycol-gentamicin sulfate microneedles. *Adv. Eng. Mater.* **2010**, *12*, B77–B82. [[CrossRef](#)]
16. Maruo, S.; Ikuta, K.; Korogi, H. Force-controllable, optically driven micromachines fabricated by single-step two-photon microstereolithography. *J. Microelectromechanical Syst.* **2003**, *12*, 533–539. [[CrossRef](#)]
17. Galajda, P.; Ormos, P. Complex micromachines produced and driven by light. *Appl. Phys. Lett.* **2001**, *78*, 249–251. [[CrossRef](#)]
18. Von Freymann, G.; Ledermann, A.; Thiel, M.; Staude, I.; Essig, S.; Busch, K.; Wegener, M. Three-dimensional nanostructures for photonics. *Adv. Funct. Mater.* **2010**, *20*, 1038–1052. [[CrossRef](#)]
19. Klein, S.; Barsella, A.; Leblond, H.; Bulou, H.; Fort, A.; Andraud, C.; Lemerrier, G.; Mulatier, J.C.; Dorkenoo, K. One-step waveguide and optical circuit writing in photopolymerizable materials processed by two-photon absorption. *Appl. Phys. Lett.* **2005**, *86*, 211118. [[CrossRef](#)]
20. Lindenmann, N.; Balthasar, G.; Hillerkuss, D.; Schmogrow, R.; Jordan, M.; Leuthold, J.; Freude, W.; Koos, C. Photonic wire bonding: A novel concept for chip-scale interconnects. *Opt. Express* **2012**, *20*, 17667. [[CrossRef](#)]
21. Zhang, S.; Tang, S.-J.; Feng, S.; Xiao, Y.-F.; Cui, W.; Wang, X.; Sun, W.; Ye, J.; Han, P.; Zhang, X.; et al. High-Q Polymer Microcavities Integrated on a Multicore Fiber Facet for Vapor Sensing. *Adv. Opt. Mater.* **2019**, *7*, 1900602. [[CrossRef](#)]
22. Ams, M.; Marshall, G.D.; Dekker, P.; Piper, J.A.; Withford, M.J. Ultrafast laser written active devices. *Laser Photonics Rev.* **2009**, *3*, 535–544. [[CrossRef](#)]
23. Tomazio, N.B.; De Boni, L.; Mendonça, C.R. Low threshold Rhodamine-doped whispering gallery mode microlasers fabricated by direct laser writing. *Sci. Rep.* **2017**, *7*, 8559. [[CrossRef](#)]
24. Li, L.; Gershgoren, E.; Kumi, G.; Chen, W.-Y.; Ho, P.-T.; Herman, W.N.; Fourkas, J.T. High-performance microring resonators fabricated with multiphoton absorption polymerization. *Adv. Mater.* **2008**, *20*, 3668–3671. [[CrossRef](#)]
25. Liu, Z.P.; Li, Y.; Xiao, Y.-F.; Li, B.-B.; Jiang, X.-F.; Qin, Y.; Feng, X.-B.; Yang, H.; Gong, Q. Direct laser writing of whispering gallery microcavities by two-photon polymerization. *Appl. Phys. Lett.* **2010**, *97*, 211105. [[CrossRef](#)]
26. Grossmann, T.; Schleede, S.; Hauser, M.; Beck, T.; Thiel, M.; von Freymann, G.; Mappes, T.; Kalt, H. Direct laser writing for active and passive high-Q polymer microdisks on silicon. *Opt. Express* **2011**, *19*, 11451. [[CrossRef](#)] [[PubMed](#)]
27. Tomazio, N.B.; Paula, K.T.; Henrique, F.R.; Andrade, M.B.; Roselló-Mechó, X.; Delgado-Pinar, M.; Andrés, M.V.; Mendonça, C.R. Mode cleaning in graphene oxide-doped polymeric whispering gallery mode microresonators. *J. Mater. Chem. C Mater.* **2020**, *8*, 9707–9713. [[CrossRef](#)]
28. Pöllinger, M.; O’Shea, D.; Warken, F.; Rauschenbeutel, A. Ultrahigh-Q Tunable Whispering-Gallery-Mode Microresonator. *Phys. Rev. Lett.* **2009**, *103*, 053901. [[CrossRef](#)]

29. Savchenkov, A.A.; Ilchenko, V.S.; Matsko, A.B.; Maleki, L. Tunable filter based on whispering gallery modes. *Electron. Lett.* **2003**, *39*, 389. [[CrossRef](#)]
30. Ioppolo, T.; Ayaz, U.; Ötügen, M.V. Tuning of whispering gallery modes of spherical resonators using an external electric field. *Opt. Express* **2009**, *17*, 16465. [[CrossRef](#)] [[PubMed](#)]
31. Adolphson, M.; Qavi, A.J.; Shmuylovich, L.; Liao, J.; Amarasinghe, G.K.; Yang, L. Reverse tuning of whispering gallery mode microresonators. In *Optics and Biophotonics in Low-Resource Settings IX*; Levitz, D., Ozcan, A., Eds.; SPIE: Bellingham, WA, USA, 2023; p. 38. [[CrossRef](#)]
32. Wang, Z.; Mallik, A.K.; Wei, F.; Wang, Z.; Rout, A.; Wu, Q.; Semenova, Y. Enhancing the thermo-optic tuning performance of whispering gallery modes in a microcapillary resonator filled with nematic liquid crystal. *Opt. Commun.* **2023**, *537*, 129442. [[CrossRef](#)]
33. Kovach, A.; He, J.; Saris, P.J.G.; Chen, D.; Armani, A.M. Optically tunable microresonator using an azobenzene monolayer. *AIP Adv.* **2020**, *10*, 045117. [[CrossRef](#)]
34. Weber, M.J. *Handbook of Optical Materials*; CRC Press: Boca Raton, FL, USA, 2018. [[CrossRef](#)]
35. Barreda, A.; Zou, C.; Sinelnik, A.; Menshikov, E.; Sinev, I.; Pertsch, T.; Staude, I. Tuning and switching effects of quasi-BIC states combining phase change materials with all-dielectric metasurfaces. *Opt. Mater Express* **2022**, *12*, 3132. [[CrossRef](#)]
36. Izdebskaya, Y.V.; Yang, Z.; Shvedov, V.G.; Neshev, D.N.; Shadrivov, I.V. Multifunctional Metasurface Tuning by Liquid Crystals in Three Dimensions. *Nano Lett.* **2023**, *23*, 9825–9831. [[CrossRef](#)] [[PubMed](#)]
37. Izdebskaya, Y.V.; Yang, Z.; Liu, M.; Choi, D.-Y.; Komar, A.; Neshev, D.N.; Shadrivov, I.V. Magnetic tuning of liquid crystal dielectric metasurfaces. *Nanophotonics* **2022**, *11*, 3895–3900. [[CrossRef](#)]
38. Birks, T.A.; Li, Y.W. The shape of fiber tapers. *J. Light. Technol.* **1992**, *10*, 432–438. [[CrossRef](#)]
39. Arkema Sartomer Americas. SR399. Available online: https://americas.sartomer.arkema.com/en/product-finders/product/f/sartomer_MonomerAcrylates_US/p/sr399/ (accessed on 31 January 2024).
40. Derkowska-Zielinska, B.; Krupka, O.; Smokal, V.; Grabowski, A.; Naparty, M.; Skowronski, L. Optical properties of disperse dyes doped poly(methyl methacrylate). *Mol. Cryst. Liq. Cryst.* **2016**, *639*, 87–93. [[CrossRef](#)]
41. Couto, F.A.; Andrade, M.B.; Otuka, A.J.G.; Pratavieira, S.; Muniz, S.R.; Mendonça, C.R. Integrating Fluorescent Nanodiamonds into Polymeric Microstructures Fabricated by Two-Photon Polymerization. *Nanomaterials* **2023**, *13*, 2571. [[CrossRef](#)] [[PubMed](#)]
42. Carmon, T.; Yang, L.; Vahala, K.J. Dynamical thermal behavior and thermal self-stability of microcavities. *Opt. Express* **2004**, *12*, 4742. [[CrossRef](#)]
43. Dong, C.-H.; He, L.; Xiao, Y.-F.; Gaddam, V.R.; Ozdemir, S.K.; Han, Z.-F.; Guo, G.-C.; Yang, L. Fabrication of high-Q polydimethylsiloxane optical microspheres for thermal sensing. *Appl. Phys. Lett.* **2009**, *94*, 231119. [[CrossRef](#)]
44. Deng, Y.; Liu, F.; Leseman, Z.C.; Hossein-Zadeh, M. Thermo-optomechanical oscillator for sensing applications. *Opt. Express* **2013**, *21*, 4653. [[CrossRef](#)]
45. Bhattacharya, S.; Veluthandath, A.V.; Murugan, G.S.; Bisht, P.B. Temperature dependence of whispering gallery modes of quantum dot-doped microbottle resonators. *J. Lumin.* **2020**, *221*, 117050. [[CrossRef](#)]
46. Goods, S. *Thermal Expansion and Hydration Behavior of PMMA Moulding Materials for LIGA Applications*; Sandia National Lab.: Albuquerque, NM, USA; Livermore, CA, USA, 2003. [[CrossRef](#)]
47. Bednarski, H.; Hajduk, B. Dispersion of thermo-optic coefficient of optical polymers. *Polymer* **2021**, *230*, 124074. [[CrossRef](#)]

Disclaimer/Publisher's Note: The statements, opinions and data contained in all publications are solely those of the individual author(s) and contributor(s) and not of MDPI and/or the editor(s). MDPI and/or the editor(s) disclaim responsibility for any injury to people or property resulting from any ideas, methods, instructions or products referred to in the content.